

Article

Petrogenesis of Garnet Clinopyroxenite and Associated Dunite in Hujialin, Sulu Orogenic Belt, Eastern China

Jianguo Liu ¹, Jian Wang ^{2,*}, Keiko Hattori ³ and Zeli Wang ⁴

¹ School of Resources and Environmental Engineering, Shandong University of Technology, Zibo 255000, China; liujg@sdut.edu.cn

² College of Earth Sciences, Jilin University, Changchun 130061, China

³ Department of Earth and Environmental Sciences, University of Ottawa, Ottawa, ON K1N 6N5, Canada; khattori@uottawa.ca

⁴ College of Earth Science and Engineering, Shandong University of Science and Technology, Qingdao 266590, China; wangze_li@126.com

* Correspondence: wangjian304@jlu.edu.cn

Abstract: The origin of ultramafic rocks, especially those in suture zones, has been a focus because they are not only important mantle sources of magma, but also provide substantial information on metamorphism and melt/fluid–peridotite interaction. Ultramafic rocks in Hujialin, in the central part of the Sulu orogen, include peridotite and pyroxenite. Although many papers on their origin and tectonic evolution have been published in the past few decades, these questions are still highly debated. Here, we present mineralogy, mineral composition, and bulk-rocks of these ultramafic rocks to evaluate their origin and tectonic evolution. The garnet clinopyroxenite is low in heavy rare-earth elements (HREE, 5.97–10.6 ppm) and has convex spoon-shaped chondrite-normalized REE patterns, suggesting the garnet formed later, and its precursor is clinopyroxenite. It is high in incompatible elements (i.e., Cs, Rb, Ba) and shows negative to positive U, Nb, and Ta anomalies, without pronounced positive Sr or Eu anomalies. Clinopyroxene in garnet clinopyroxenite contains high MgO (Mg[#] 0.90–0.97). The mineral chemistry and bulk-rock compositions are similar to those of reactive clinopyroxenite, suggesting that it originally formed via peridotite–melt interaction, and that such silicic and calcic melt might derive from the subducted Yangtze continent (YZC). Dunite contains olivine with high Fo (93.0–94.1), low NiO (0.11–0.29 wt.%) and MnO (≤0.1 wt.%), chromite with high Cr[#] (0.75–0.96), TiO₂ (up to 0.88 wt.%), and Na₂O (0.01–0.10 wt.%). It has negatively sloped chondrite-normalized REE patterns. Mineral chemistry and bulk rocks suggest dunite likely represent residual ancient lithospheric mantle peridotite beneath the North China Craton (NCC) that was overprinted by aqueous fluids. The lack of prograde and retrograde metamorphic minerals in dunite and irregular shaped mineral inclusions in chromite suggest dunite did not subduct to deep levels. Dunite mingled with garnet clinopyroxenite during exhumation of the latter at shallow depths. These ultramafic rocks, especially hydrated peridotite, may be important sources of Au for the Jiaodong gold province in the NCC.

Keywords: Sulu orogenic belt; clinopyroxenite; North China Craton; melt–peridotite interaction



Citation: Liu, J.; Wang, J.; Hattori, K.; Wang, Z. Petrogenesis of Garnet Clinopyroxenite and Associated Dunite in Hujialin, Sulu Orogenic Belt, Eastern China. *Minerals* **2022**, *12*, 162. <https://doi.org/10.3390/min12020162>

Academic Editors: Hafiz U. Rehman, Atsushi Kamei, Clemente Recio and Yaoling Niu

Received: 16 December 2021

Accepted: 25 January 2022

Published: 28 January 2022

Publisher's Note: MDPI stays neutral with regard to jurisdictional claims in published maps and institutional affiliations.



Copyright: © 2022 by the authors. Licensee MDPI, Basel, Switzerland. This article is an open access article distributed under the terms and conditions of the Creative Commons Attribution (CC BY) license (<https://creativecommons.org/licenses/by/4.0/>).

1. Introduction

The Dabie-Sulu orogenic belt formed from the subduction of Yangtze Craton (YZC) beneath the North China Craton (NCC) in the Triassic in east-central China [1–3]. It is one of the largest ultrahigh-pressure (UHP) metamorphic terranes in the world with an exposed area of about 30,000 km² [4,5]. The terrane is mainly composed of granitic gneisses, with volumetrically minor ultramafic rocks occurring as massifs and lenticular bodies. These ultramafic rocks include garnet peridotite, spinel peridotite, and pyroxenite. They mainly distribute in Weihai, Rongcheng (Chijiadian, Lijiatun, and Macaokuang), Jiangzhuang, Xugou, Rizhao (Suoluoshu and Hujialin), and Yangkou [1,2,6] (Figure 1a).

Ultramafic rocks in Hujialin are surrounded by granitic gneiss, and mainly consist of serpentinized peridotite with minor dunite and clinopyroxenite lenses [7]. The origin of pyroxenite has been a focus not only because pyroxenite subducted into the mantle is an important source for magma, but also because the pyroxenite returned to the surface provides substantial information on metamorphism and melt/fluid–peridotite interaction [8]. Although many papers on the origin of Hujialin clinopyroxenite have been published in the past few decades, the question of whether the clinopyroxenite is a cumulate of magma [7,9–11] or a product of melt–peridotite interaction [12] is still highly debated. Besides, given that clinopyroxenite occurs closely associated with dunite somewhere in Hujialin [5], questions such as “What is the relationship between their origins?” and “How did they exhume together?” require further discussion.

This study presents detailed petrology, mineral composition, and bulk-rock geochemistry of clinopyroxenite and dunite of Hujialin, to evaluate the origin and tectonic evolutions of these two ultramafic rocks.

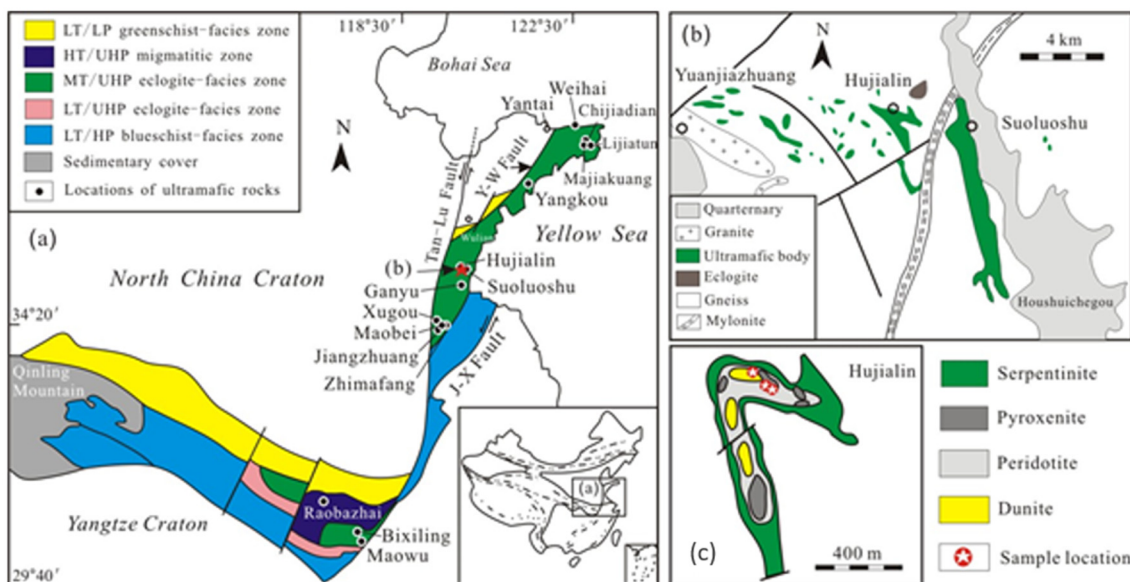


Figure 1. (a) A sketch map showing the framework of the Dabie-Sulu orogenic belt and the distribution of orogenic ultramafic rocks (modified after Zheng et al. [13]; Chen et al. [14]). (b) Geological sketch map of the Rizhao area, showing the position of ultramafic rocks in Hujialin (modified after Zhang and Liou [15]). (c) Outcrop map of the Hujialin ultramafic rocks (after Zhang and Liou [15]). Abbreviations: Y-W Fault = Yantai-Wulian Fault; J-X Fault = Jiashan-Xiangshui Fault.

2. Geological Setting

The Sulu orogen is displaced northward from the Dabie orogen by the sinistral Tan-Lu fault for about 500 km. It is bounded by the Yantai-Wulian to the north, and Jiashan-Xiangshui fault to the south (Figure 1a). Three main fault-bounded metamorphic zones are classified, with (I) low-temperature/low-pressure (LT/LP) greenschist-facies zone in the north composed of Neoproterozoic igneous rocks and Neoproterozoic-pre-Triassic sedimentary rocks; (II) mid-temperature/ultrahigh-pressure (MT/UHP) eclogite-facies zone in the central dominated by ortho- and paragneiss with layers and blocks of eclogite, amphibolite, marble, and sporadically distributed ultramafic bodies; and (III) low-temperature/high-pressure (LT/HP) blueschist-facies zone in the south consisting of quartzite schist, ortho- and paragneiss, marble, and blueschist [16–19]. They are unconformably overlain by Jurassic siliciclastic and Cretaceous volcanoclastic rocks and intruded by post-orogenic Mesozoic granites [19].

The rocks in UHP zones retain evidence of UHP metamorphism, such as coesite inclusions in minerals of garnet, omphacite, jadeite, kyanite, and epidote from both eclogite

and metasedimentary rock in Donghai area [16]; the presence of exsolved clinopyroxene, rutile, and apatite in garnet from Yangkou eclogite [20], and coesite and other ultrahigh-pressure mineral inclusions in zircon from eclogite and gneiss core samples of the Chinese Continental Scientific Drilling Site (CCSD) [19,21,22]. This indicates that both supracrustal and basement rocks underwent UHP metamorphism at subarc depths more than 100 km. U-Pb zircon dating of garnet peridotites [23], UHP gneisses [24], and eclogites [25] shows that they were subjected to UHP metamorphism at 245–220 Ma. The peak metamorphic conditions were considered to be 750–850 °C and 3.4–4.0 GPa [19].

The Hujialin ultramafic complex is situated in Rizhao City and located in the middle of the Sulu orogen. It trends NNW-SSE for about 6 km long and is cut by a NE-SW-trending fault (Figure 1b). The ultramafic complex is in fault contact with the UHP gneiss. It mainly consists of serpentinized peridotite that contains minor discontinuous lenses of garnet clinopyroxenite and dunite (Figure 1c). Petrological studies, such as mineral exsolution texture in clinopyroxene, mineral assemblage, and associated P-T calculation, indicate that the Hujialin garnet clinopyroxenite underwent UHP metamorphism [5,15,26]. Zircons discovered from the ultramafic complex yielded U-Pb ages of 215–226 Ma, consistent with the time of initial exhumation of deeply subducted continental crust in the Dabie-Sulu orogenic belt [27–29]. Some spinel peridotites show no evidence of UHP metamorphism and may have undergone different paths [2,11].

3. Materials and Methods

3.1. Sample Description

We examined nine clinopyroxenite samples and six dunite samples. They were collected in the northern lenses of the Hujialin complex in a stone pit (Figure 1c), with eight clinopyroxenite samples at 35°12'24" N, 119°15'6" E; one clinopyroxenite (HJ-19) at 35°12'23" N, 119°15'8" E; and dunite at 35°12'35" N, 119°15'2" E. The Hujialin complex is not very large, and the pyroxenite and dunite are mainly exposed in the northern part of the complex based on our field observation. Therefore, the samples that we collected may represent the whole set of outcrops of pyroxenite-dunite.

Clinopyroxenite is divided into omphacite-bearing (type-1, samples of HJ-1, HJ-6) and omphacite-free (type-2) varieties. Type-2 clinopyroxenite is subdivided into garnet-rich (type-2A, samples of HJ-8, HJ-16) and garnet-poor (type-2B, samples of HJ-2, HJ-9, HJ-10, HJ-12, HJ-19) varieties. Type-1 and type-2A clinopyroxenite are partly altered and show porphyroblastic texture, in which coarse-grained garnet (20–50 vol.%, 1.5–5 mm in size) occurs in a fine-grained matrix (0.4 mm on average) that is composed of garnet (~10 vol.%), clinopyroxene with minor alteration minerals (amphibole, chlorite, and epidote), and Fe-oxides (magnetite and ilmenite) (Figure 2a,b). Clinopyroxene, including omphacite (euhedral to anhedral, 35–65 vol.%) occurs as inclusions in garnet and isolated grains (Figure 2c). Clinopyroxene shows an interlocking texture with fine-grained garnet and has irregular boundaries. It is euhedral to subhedral in sample of HJ-8, and sometimes shows 120° triple junction (Figure 2d). In sample of HJ-16, clinopyroxene grains are elongated and show preferred orientation (Figure 2e). Fe-oxide intergrowths in type-1 clinopyroxenite (commonly <0.2 mm in size, <2 vol.%) mainly occur in interstitial spaces of other minerals and are enclosed in clinopyroxene and occasionally in garnet.

Type-2B clinopyroxenite is moderately altered and shows equigranular texture, except for HJ-9, which shows porphyroblastic texture. Garnet-poor clinopyroxenite contains clinopyroxene (euhedral to anhedral, 0.5 mm on average, >90 vol.%), garnet (<1 mm in size, ~5 vol.%), alteration minerals (amphibole, chlorite, and epidote), Fe-oxides (magnetite, and ilmenite), and titanite (Figure 2f). Clinopyroxene occurs as inclusions in garnet and isolated grains in matrix. In HJ-9, coarse-grained clinopyroxene (~1 mm in size) is commonly surrounded by fine-grained clinopyroxene (~0.1 mm). Garnet commonly contains clinopyroxene inclusions and occasionally contains amphibole and Fe-oxides (Figure 2g). It is mostly altered and rimmed by amphibole, epidote, and chlorite (Figure 2f). Similar to garnet-rich clinopyroxenite, Fe-oxides and titanite intergrowths (commonly <0.2 mm in

size, <2 vol.%) mainly occur in interstitial spaces of other minerals (Figure 2h,i). A grain (irregular in shape and 0.4 mm in size) showing chromite and ilmenite intergrowth was discovered in interstitial space of clinopyroxene in sample HJ-10.

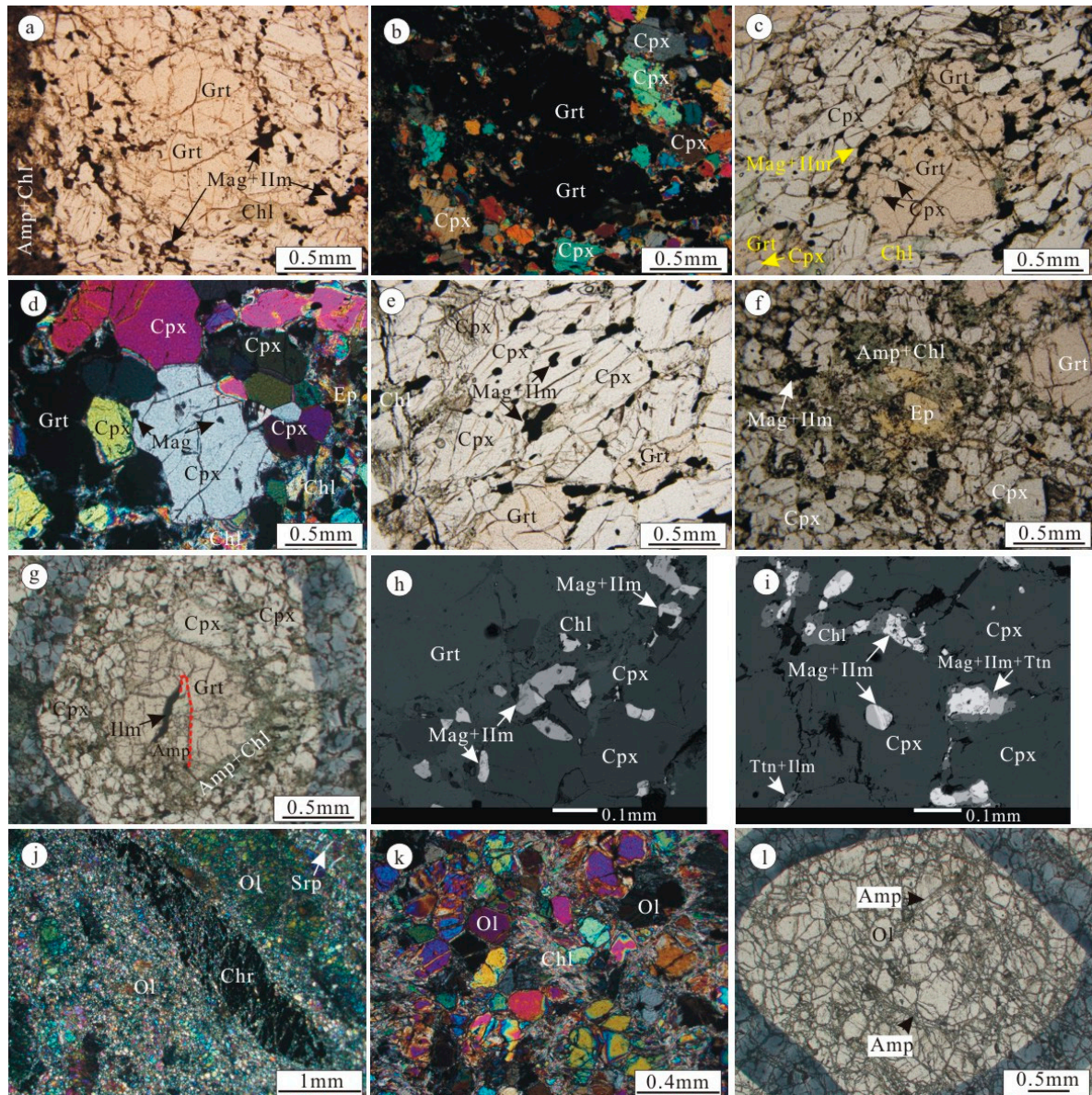


Figure 2. Photomicrographs of garnet pyroxenite and dunite at Hujialin in the Sulu orogen, showing mineral assemblages and characteristic textures. (a,b) Type-1 and type-2A clinopyroxenite show porphyroblastic texture. (c) Clinopyroxene occurs as inclusions in garnet and isolated grains. (d) Euhedral to anhedral clinopyroxene. (e) Clinopyroxene grains are elongated and show preferred orientation in some samples. (f) Garnet-poor clinopyroxenite composed of clinopyroxene, garnet, alteration minerals, Fe-oxides, and titanite. (g) Clinopyroxene, minor amphibole, and Fe-oxides are included in garnet. (h,i) Fe-oxides and titanite intergrowths occur in interstitial spaces of other minerals. (j–l) Dunite consists of olivine and chromite. Some chromite grains show preferred orientation. Amp = amphibole; Chl = chlorite; Chr = chromite; Cpx = clinopyroxene; Ep = epidote; Grt = garnet; Ilm = ilmenite; Mag = magnetite; Ol = olivine; Srp = serpentine; Ttn = titanite. Mineral abbreviations after Whitney and Evans [30].

Dunite (samples of HJ-20, HJ-23, HJ-25, HJ-27, HJ-28, and HJ-29) is slightly to moderately altered along cracks and boundaries of olivine into serpentine, amphibole, and

chlorite (Figure 2j–l). It shows a granular mosaic structure, and mainly consists of olivine (~0.6 mm in size, >95 vol.%) and chromite (<3 vol.%). No sulfide minerals are found. Some olivine and chromite grains are mylonitized and show preferred orientation (Figure 2j). Chromite shows uneven size (<0.1 mm to 2 mm) and varying color (dark red to opaque). It occurs in interstitial spaces of olivine grains. Several chromite grains form aggregates.

3.2. Analytical Methods

Mineral compositions were determined using a JEOL JXA-8230 microprobe by the wavelength dispersive method at the Institute of Mineral Resources, Chinese Academy of Geological Sciences, Beijing, China. The peak counting time was 10 s for each element. Analytical conditions were 15 kV accelerating voltage, 20 nA beam current, and 5 μm beam spot. The standards were jadite (Si, Al, Na), forsterite (Mg), rutile (Ti), topaz (F), potash feldspar (K), wollastonite (Ca), hematite (Fe), Cr_2O_3 (Cr), MnO (Mn), NiO (Ni), and NaCl (Cl). Raw data were corrected using a ZAF program. Fe^{3+} and Fe^{2+} contents of chromite were calculated based on stoichiometry of AB_2O_4 .

Samples were crushed to powders of 2 μm in agate mortars for bulk-rock major and minor elements analysis in Yanduzhongshi Geological Analysis Laboratories Ltd., Beijing, China. Bulk-rock major elements were analyzed by an X-ray fluorescent spectrometer (XRF-1800). Bulk-rock powder was added to a flux of lithium metaborate, mixed well, and fused in a furnace at 1150 $^\circ\text{C}$. A flat glass disk was prepared, and then the major elements were analyzed by XRF. Relative standard deviations for major element oxides are within 1%.

Minor elements were analyzed by inductively coupled mass spectrometry (ICP-MS, M90). The sample preparation procedure was similar to that described by Li et al. [12]. Sample powder was heated in an oven at 105 $^\circ\text{C}$ for 12 h, and 50 mg of powder was weighed and placed into Teflon bombs with a mixture of HF and HNO_3 . The Teflon bomb was put in a stainless-steel pressure jacket and heated to 190 $^\circ\text{C}$ for 24 h. After cooling, the Teflon bomb was opened and placed on a hotplate at 140 $^\circ\text{C}$ and evaporated to incipient dryness. Then, 1 mL HNO_3 , 1 mL MQ water, and 1 mL internal standard solution of 1 ppm In was added. The Teflon bomb was resealed and put in the oven at 190 $^\circ\text{C}$ for >12 h. The final solution was transferred to a polyethylene bottle and diluted to 100 g by 2% HNO_3 for ICP analysis. Standards of AGV-2, BHVO-2, BCR-2, BGM-2, and GSR-2 were used to monitor the analytical quality. Relative standard deviations for most minor elements are within 5%.

4. Results

4.1. Mineral Chemistry

4.1.1. Clinopyroxene and Garnet in Clinopyroxenite

Clinopyroxene is diopside and omphacite in type-1 clinopyroxenite (Supplementary Materials Table S1, Figure 3). Omphacite inclusions contain slightly higher Jd content ($=100 \times \text{Al}^{\text{VI}} / (\text{Na} + \text{Ca})$) of 29–30 mol% than isolated ones (26–28 mol%), both of which are similar to the composition of omphacite from eclogite in Sulu orogen [31,32] (Figure 3). The composition of diopsidic clinopyroxene is not listed in Supplementary Materials Table S1 because of its slightly low total content (SiO_2 52.9 wt.%, TiO_2 0.12 wt.%, Al_2O_3 2.57 wt.%, Cr_2O_3 0.04 wt.%, FeO 2.96 wt.%, MnO < 0.01 wt.%, MgO 13.9 wt.%, CaO 23.8 wt.%, Na_2O 0.33 wt.%, K_2O < 0.01 wt.%, with total content 96.6 wt.%).

Diopside in type-2 clinopyroxenite contains high MgO (15.7–17.6 wt.%) with $\text{Mg}^\#$ ($=\text{Mg}^{2+} / (\text{Mg}^{2+} + \text{Fe}_{\text{total}})$) 0.90–0.97, SiO_2 (53.1–56.3 wt.%), low TiO_2 (<0.25 wt.%), Na_2O (0.38–0.94 wt.%), and Al_2O_3 (0.72–3.13 wt.%). Diopside inclusions have identical composition with isolated grains (Supplementary Materials Table S1). The composition is close to that of diopside in mantle peridotite of the North China Craton (Figure 4). The diopside studied here shows little exsolved phases and is likely close to the composition at the time of crystallization.

Garnet shows variable proportions of pyrope, grossular, and almandine components. It is represented by $\text{Prp}_{19-25}\text{Alm}_{22-26}\text{Gro}_{48-57}$, $\text{Prp}_{28-38}\text{Alm}_{21-24}\text{Gro}_{41-49}$, and $\text{Prp}_{28-42}\text{Alm}_{20-30}\text{Gro}_{34-47}\text{Spe}_{0-1}$ (Prp: pyrope; Alm: almandine; Gro: grossular; Spe: spessartine) in type-1, type-2A, and type-2B clinopyroxenite, respectively, similar to the B-type and C-type garnet defined by Coleman et al. [33] (Supplementary Materials Table S2, Figure 5). The Si content of garnet is generally >6 apfu, suggesting the Hujialin garnet clinopyroxenite underwent UHP metamorphism as documented by Zhang and Liou [15].

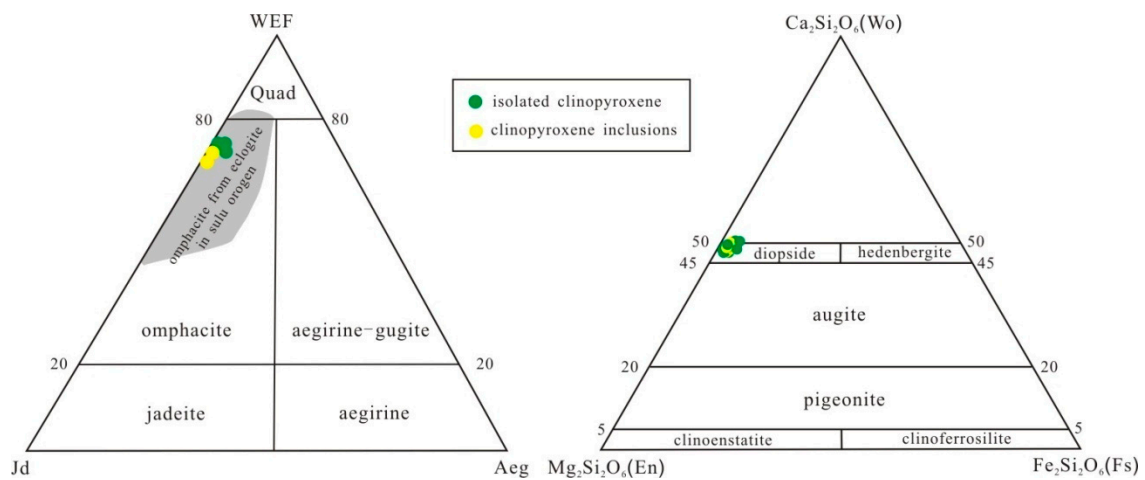


Figure 3. Classification diagrams for clinopyroxene [34]. Jd (Jadeite) = $100 \times \text{Al}^{\text{VI}}/(\text{Na} + \text{Ca})$, Aeg (Aegirine) = $100 \times (\text{Na} - \text{Al}^{\text{VI}})/(\text{Na} + \text{Ca})$, WEF (wollastonite + enstatite + ferrosilite) = $100 - \text{Jd} - \text{Ae}$.

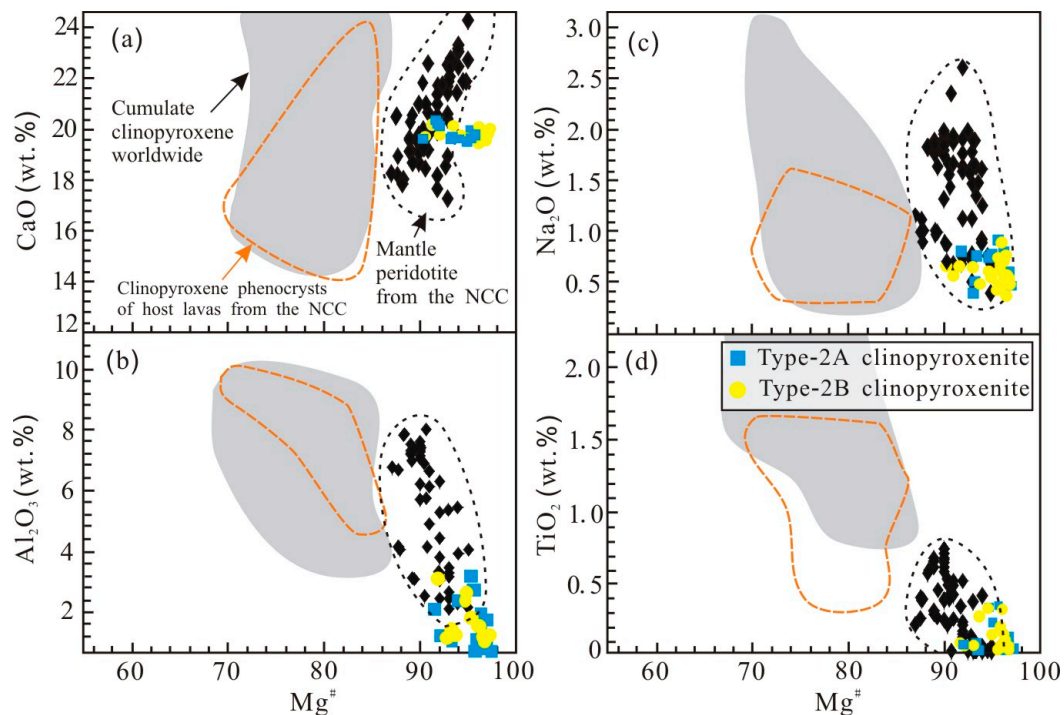


Figure 4. Major element oxides variation diagrams of clinopyroxene in Hujialin type-2 clinopyroxenite (a) CaO; (b) Na₂O; (c) Al₂O₃; (d) TiO₂. Data sources: cumulate clinopyroxene worldwide is based on Liu and Ying [35] and references therein; field of clinopyroxene phenocrysts of host lavas from the North China Craton (NCC) is from Xu et al. [36], and Liu and Ying [35]; mantle peridotite from the NCC is from the Zheng et al. [37,38], Ying et al. [39], and Xu et al. [36,40].

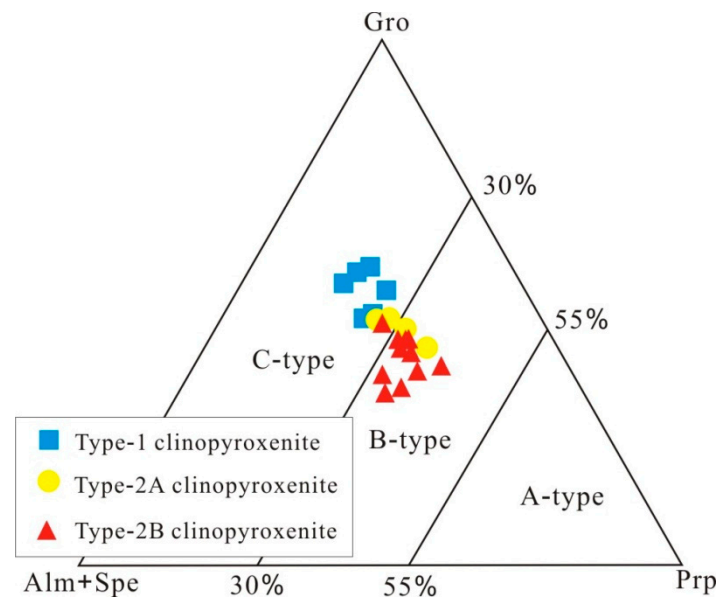


Figure 5. Composition of garnet. Three types of garnet are after Coleman et al. [33].

4.1.2. Olivine and Chromite in Dunite

Olivine in dunite has consistently high Fo ($Fo = 100 \times Mg/[Mg + Fe]$; 93.0–94.1), and low NiO (0.11–0.29 wt.%) and MnO (≤ 0.1 wt.%) (Supplementary Materials Table S3). The Fo for studied samples is comparable to that of mantle olivine and ancient sub-continental lithospheric mantle (SCLM), but the NiO and MnO are both lower than those of mantle olivine, ancient SCLM, and Cenozoic SCLM (Figure 6).

Chromite contains high $Cr^\#$ ($=Cr/[Cr + Al]$; 0.75–0.96), relatively high TiO_2 (up to 0.88 wt.%) and Na_2O (0.01–0.10 wt.%), and low XFe^{3+} ($=Fe^{3+}/[Fe^{3+} + Al + Cr]$; ≤ 0.18) (Supplementary Materials Table S4). It is not homogeneous in composition within individual grains, with higher Cr, Mg, and Al and lower Fe in cores (Cr_2O_3 52.3–60.0 wt.%, MgO 4.98–8.40 wt.%, Al_2O_3 5.52–12.5 wt.%, FeO 20.8–30.0 wt.%) than in rims (Cr_2O_3 12.6–53.8 wt.%, MgO 1.20–3.83 wt.%, Al_2O_3 0.01–2.15 wt.%, FeO 36.2–70.3 wt.%) (Figure 7), similar to altered chromite in forearc mantle serpentinites of the Rio San Juan complex reported by Saumur and Hattori [41]. On a ternary diagram of Fe^{3+} -Cr-Al, and binary $Cr^\#$ -Mg and Al_2O_3 - TiO_2 diagrams, chromite plots into the fields of Himalayas and forearc peridotite (Figure 8).

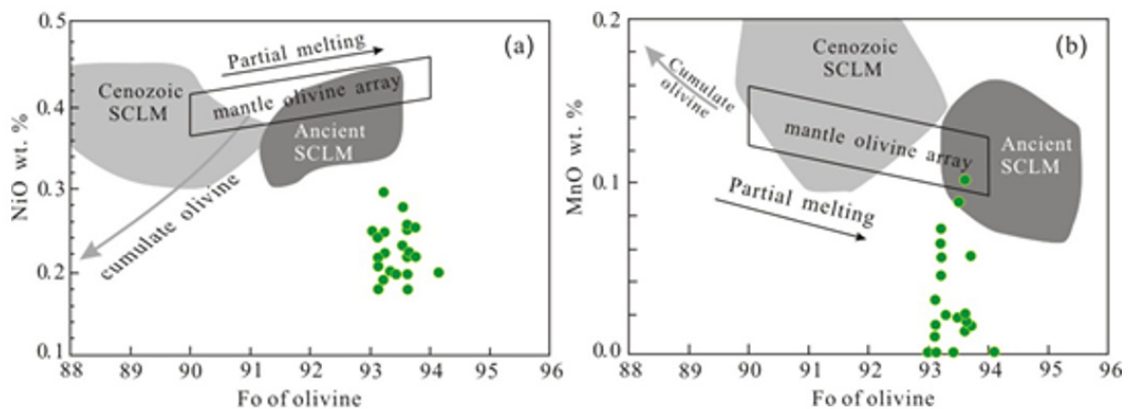


Figure 6. Compositional variations of olivine. (a) NiO vs. Fo. (b) MnO vs. Fo. The mantle olivine array is based on Hattori et al. [42]. Partial melting trend is from Ozawa [43]. Trend of cumulate olivine is from Ozawa [43] and Nakamura [44]. Fields of Ancient and Cenozoic subcontinental lithospheric mantle (SCLM) are from Xie et al. [2] and references therein.

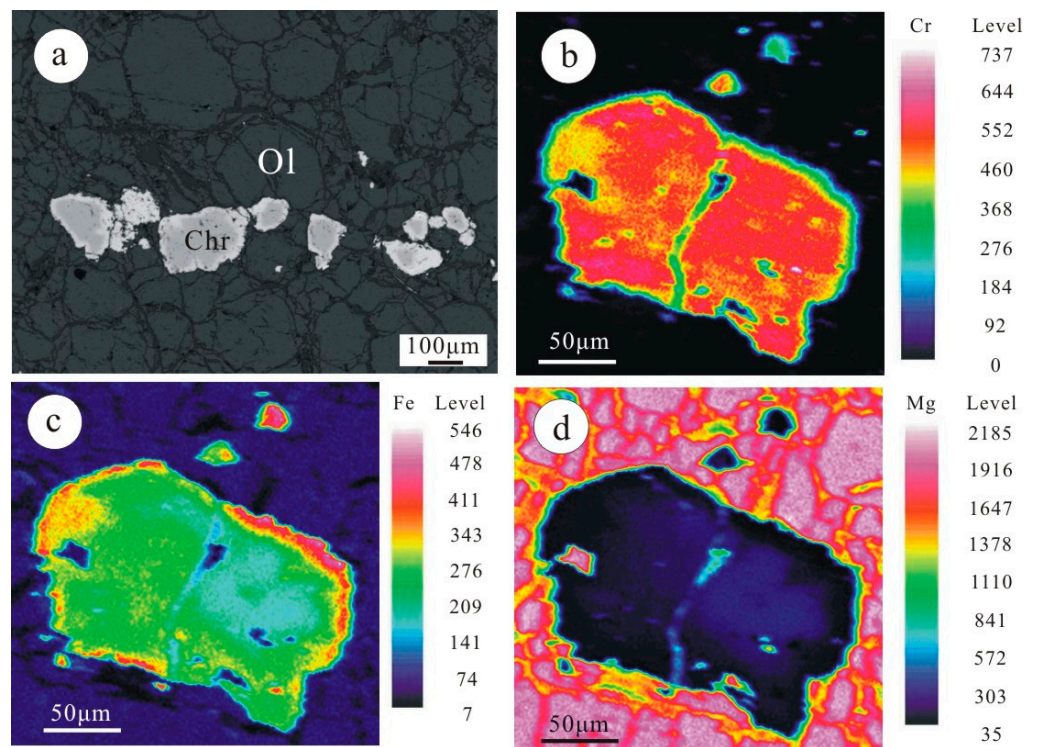


Figure 7. Back-scattered electron image of chromite in dunite (a) and distribution diagrams of elements for Cr (b), Fe (c), and Mg (d) in chromite.

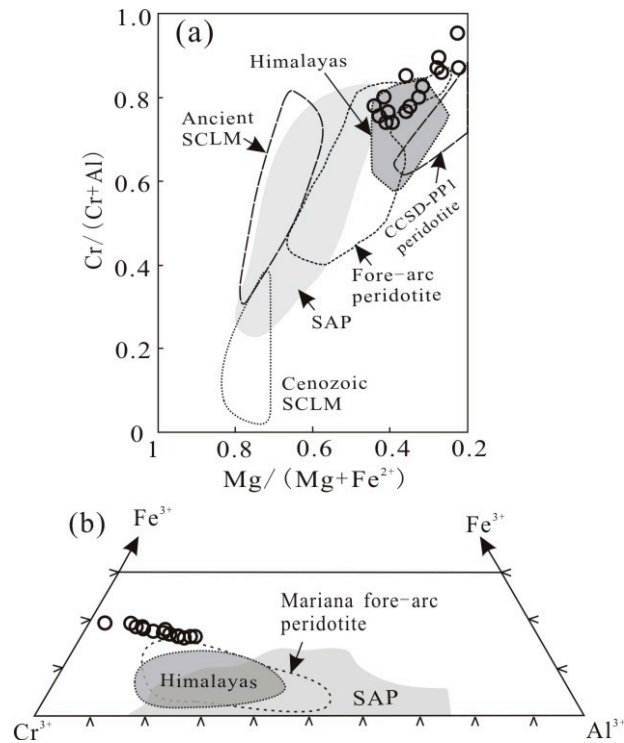


Figure 8. Plots of $Cr/(Cr + Al)$ vs. $Mg/(Mg + Fe^{2+})$ (a) and $Cr-Al-Fe^{3+}$ (b) for chromite in dunite of Hujialin. Data sources: forearc peridotite [45], Mariana fore-arc peridotite [46], Himalayan forearc mantle peridotite [47], and sub-arc peridotite (SAP) [48]. Fields of ancient and Cenozoic SCLM beneath the North China Craton, as well as CCSD-PP1 peridotite, are based on Xie et al. [2] and references therein.

4.1.3. Other Minerals

Chlorite, epidote, amphibole, and titanite occur as retrograde minerals in clinopyroxenite. Chlorite, amphibole, and serpentine occur as secondary minerals in dunite. Chlorite in different types of samples shows different composition (Supplementary Materials Table S5). It is clinochlore in type-2A clinopyroxenite with moderate SiO₂ (28.8–30.6 wt.%), Al₂O₃ (18.4–19.6 wt.%), FeO (1.91–5.19 wt.%), and MgO (29.8–31.4 wt.%). Chlorites are clinochlore and sheridanite varieties in type-2B clinopyroxenite with relatively low SiO₂ (26.8–29.1 wt.%) and MgO (24.8–29.8 wt.%), and high Al₂O₃ (19.8–21.2 wt.%) and FeO (5.67–11.17 wt.%). Chlorite in dunite contains the highest SiO₂ (35.2 wt.%) and MgO (33.3 wt.%), while the lowest Al₂O₃ (11.2 wt.%) and FeO (1.2 wt.%) belong to pennine variety.

Epidote in type-1 clinopyroxenite shows slightly lower SiO₂ (36.4–37.9 wt.%), Al₂O₃ (23.7–24.5 wt.%), and Cr₂O₃ (0.01–0.05 wt.%), and higher FeO (6.76–8.17 wt.%) relative to epidote in type-2B clinopyroxenite (SiO₂ 37.4–38.4 wt.%, Al₂O₃ 24.0–25.3 wt.%, Cr₂O₃ 0.22–0.44 wt.%, FeO 5.21–7.21 wt.%). The X_{Fe} (=Fe³⁺/(Fe³⁺ + Al + Cr + Mn)) of epidote in type-1 and type-2B clinopyroxenite is 0.06–0.13 and 0–0.08, and belongs to clinozoisite-epidote and zoisite, respectively, based on the classification of Enami et al. [49] (Supplementary Materials Table S5).

Amphibole is pargasite in clinopyroxenite and tremolite in dunite based on the classification described by Hawthorne et al. [50]. Pargasite contains SiO₂ (43.9–45.4 wt.%), Al₂O₃ (12.5–14.5 wt.%), FeO (2.91–8.50 wt.%), MgO (14.6–18.4 wt.%), CaO (10.5–12.5 wt.%), Na₂O (1.51–3.05 wt.%), and K₂O (0.47–1.80 wt.%). Tremolite contains higher SiO₂ (58.8 wt.%), MgO (24.4 wt.%), and CaO (13.0 wt.%), and lower Al₂O₃ (0.21 wt.%), FeO (0.88 wt.%), Na₂O (0.09 wt.%), and K₂O (0.02 wt.%) (Supplementary Materials Table S6).

Serpentine in dunite shows two varieties. One contains SiO₂ (41.2–43.8 wt.%), MgO (39.1–43.1 wt.%), Al₂O₃ (≤0.13 wt.%), and CaO (≤0.01 wt.%). The other type contains relatively high SiO₂ (59.3 wt.%), low MgO (29.5 wt.%), and comparable Al₂O₃ (0.14 wt.%) and CaO (0.04 wt.%) (Supplementary Materials Table S6).

4.2. Bulk-Rock Compositions

4.2.1. Major Elements

Type-1 clinopyroxenite contains lower SiO₂ (44.9–45.9 wt.%), MgO (9.38–9.74 wt.%), and CaO (17.6–17.9 wt.%), and higher Al₂O₃ (13.2–13.9 wt.%), Na₂O (1.52–2.07 wt.%), and K₂O (0.10–0.12 wt.%) relative to type-2 clinopyroxenite (SiO₂ 45.9–47.5 wt.%, MgO 12.6–14.4 wt.%, CaO 18.6–20.1 wt.%, Al₂O₃ 4.84–9.28 wt.%, Na₂O 0.46–0.63 wt.%, K₂O 0.04–0.10 wt.%) (Supplementary Materials Table S7). The compositions of them are slightly different from those of eclogite and garnet pyroxenite metamorphosed from cumulative pyroxenite (Figure 9).

Dunite contains similar contents of SiO₂ (38.2–39.8 wt.%), Fe₂O₃ (7.72–8.20 wt.%), and MnO (0.11–0.17 wt.%), higher MgO (46.6–48.8 wt.%) and Na₂O (0.02–0.04 wt.%), and lower CaO (0.05–0.35 wt.%) and TiO₂ (~0.01 wt.%) relative to that reported by Xie et al. [2].

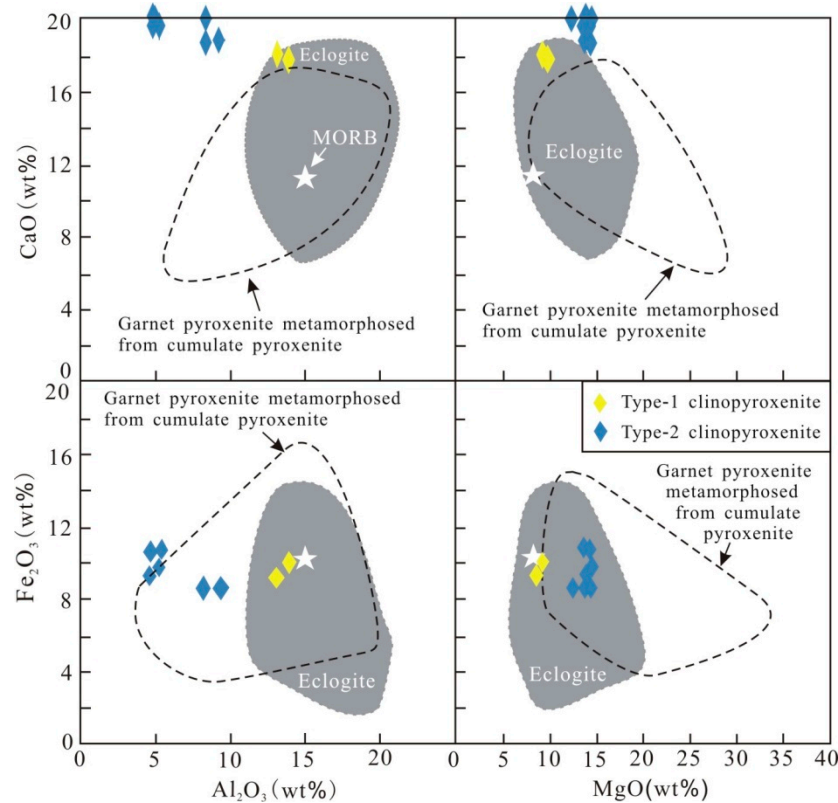


Figure 9. Ca-Fe-Al-Mg variation in eclogite and garnet pyroxenite metamorphosed from cumulate pyroxenite [51]. Average composition of MORB is based on White and Klein [52].

4.2.2. Minor Elements

Clinopyroxenite samples have similar convex-upward primitive mantle-normalized trace element patterns (Figure 10), with high concentrations of incompatible elements (i.e., Cs, Rb, Ba), negative to positive U, Nb, Ta anomalies; consistently negative Th and Zr anomalies; and positive Hf anomalies. Type-1 clinopyroxenite has no obvious Eu anomaly, negative to without Sr anomalies, and higher concentrations of REE (77.0–82.1 ppm), while type-2 clinopyroxenite shows negative Eu anomaly, negative to positive Sr anomalies, and relatively lower concentrations of REE (25.7–36.6 ppm) (Supplementary Materials Table S7, Figure 10). They have similar convex spoon-shaped chondrite-normalized REE patterns, showing enrichment from La to Nd, and depletion from Nd to Lu (Figure 10).

Dunite samples have low concentrations of trace elements as a whole (0.55–1.39 ppm) and display negatively sloped primitive mantle-normalized trace element patterns (Supplementary Materials Table S7, Figure 10). They show positive Ba, U, Ta, Pb, and Hf anomalies; negative Rb, Th, Nb, Zr anomalies, slightly positive Sr anomaly; and negative Eu anomaly (Figure 10). They display negatively sloped chondrite-normalized REE patterns and show depletion from La to Tm and flat to slight enrichment from Tm to Lu. The characteristics of dunite are similar to those of Archean cratonic mantle peridotite beneath the North China Craton (NCC) [40] and Suoluoshu serpentinite [3] (Figure 10).

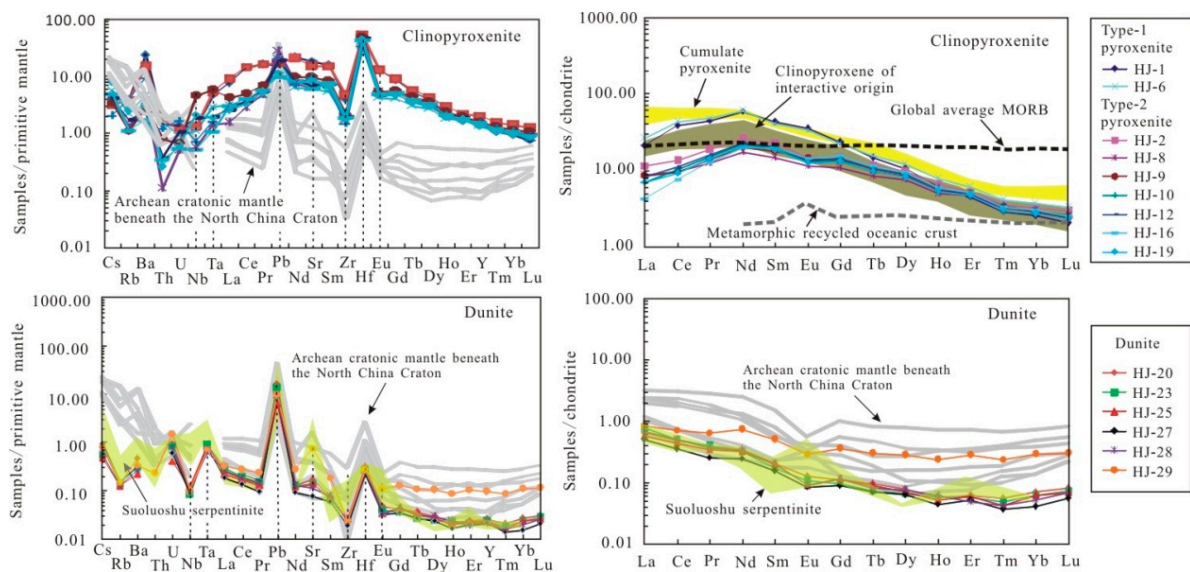


Figure 10. Primitive mantle-normalized trace elements and chondrite normalized REE for Hujialin pyroxenite and dunite in Sulu orogen. Archean cratonic mantle beneath the North China Craton [40], Suoluoshu serpentinite [3], global average MORB [52], cumulate pyroxenite [53], reactive clinopyroxene [36], and metamorphic recycled oceanic crust [54,55] are listed for comparison. Data of primitive mantle and chondrite are from McDonough and Sun [56].

5. Discussion

5.1. Origin of Hujialin Garnet Clinopyroxenite and Nature of Metasomatic Agent

Although there is a compositional overlap between eclogite and garnet pyroxenite in Ca, Fe, Al, and Mg contents, the two are not identical in origin [51,57]. Eclogite is linked to the subducted oceanic slab and has a basaltic or gabbroic precursor, while garnet pyroxenite is a cumulate of mantle-derived melt or a product of melt–peridotite interaction [36,42,51,54]. Type-1 garnet clinopyroxenite contains omphacite, high Al_2O_3 content (13.2–13.9 wt.%), and low MgO content (9.38–9.74 wt.%) relative to type-2 clinopyroxenite, and it seems to show affinity with eclogite (Figure 9); however, its trace-element features argue against this possibility. Pronounced positive Sr and Eu anomalies and flat HREE patterns are striking features of eclogite, due to its plagioclase-bearing protolith [51,57], while type-1 garnet clinopyroxenite shows no evident positive Eu or Sr anomalies and has negatively sloped HREE patterns (Figure 10). In addition, if type-1 garnet clinopyroxenite is derived from metamorphism of solid-state recycled oceanic slab, its major compositions and normalized REE patterns should be similar to those of MORB [57] (Figure 10). As illustrated in Figures 9 and 10, the high CaO content and REE patterns of type-1 garnet clinopyroxenite, together with type-2 garnet clinopyroxenite, do not resemble those of MORB and metamorphic recycled oceanic slab, indicating the Hujialin garnet clinopyroxenite is different from eclogite in origin.

The garnet clinopyroxenite samples have low concentrations of HREE (5.97–10.6 ppm, Supplementary Materials Table S7) and convex spoon-shaped chondrite-normalized REE patterns, indicating that garnet formed later during deep subduction, and the prograde metamorphic process formed in a closed system because garnet preferentially incorporates HREE [42]. If garnet was an initial phase or there was melt/fluid injected during the metamorphic process, the garnet clinopyroxenite samples would contain high concentrations of HREE [42]. This interpretation is also in agreement with the common occurrence of clinopyroxene and ilmenite inclusions in garnet. Therefore, the precursor of Hujialin garnet clinopyroxenite is clinopyroxenite.

As previously mentioned, there are two possible origins for clinopyroxenite: cumulate of a mantle-derived melt [42,51] and interactive product between melt and peridotite [36,54].

The Hujialin clinopyroxenite shows negatively sloped REE patterns and may be a cumulate from a melt. However, the clinopyroxene contains high MgO with $Mg^{\#}$ up to 0.90–0.97 (Supplementary Materials Table S1), which is distinct from that of clinopyroxene phenocrysts of host lavas worldwide (Figure 4), but similar to that of clinopyroxene of mantle peridotite from the North China Craton (Figure 4). Furthermore, Hujialin clinopyroxenite contains high CaO and the major compositions are different from those of garnet pyroxenite metamorphosed from cumulate pyroxenite (Figure 9). The REE patterns of Hujialin garnet clinopyroxenite are also different from those of cumulate pyroxenite, but similar to those of clinopyroxene of reactive origin, because cumulate pyroxenite has almost flat LREE and HREE patterns (Figure 10). Therefore, we propose the protolith of Hujialin garnet clinopyroxenite is not a cumulate of a mantle-derived melt. Instead, it is a product of melt–peridotite interaction, which is also supported by the relic olivine grains with rounded and eroded shapes included in clinopyroxene [27].

The findings above raise the question of the nature of the metamorphic melt. The replacement of olivine by clinopyroxene indicates the metamorphic agent is a silicic and calcic melt, and the transformation from olivine to clinopyroxene may have involved two reactions: (1) olivine + SiO_2 (melt₁) = orthopyroxene (+melt₂), and (2) orthopyroxene + Ca (melt₃) = clinopyroxene (+melt₄), similar to the formation of websterite xenoliths from the Feixian basalts in the eastern NCC [36]. Petrographic observations of calcite in matrix, dolomite in porphyroblastic garnet [12], and high CaO content of bulk-rock composition (Figure 9) support the involvement of a carbonatitic melt. Such a silicic and calcic melt may derive from the Yangtze continent during its subduction beneath the North China Craton. Therefore, the studied samples were primarily formed from peridotite-silicic and calcic melt interaction, which were later transformed to garnet clinopyroxenite during deep subduction of the Yangtze continent.

5.2. Origin of Dunite

There are three possible origins for dunite: (1) cumulate of a mafic melt [58], (2) reactive product of peridotite and silicon-unsaturated mafic melt [59], and (3) residue after partial melting [42].

Dunite contains relatively high concentrations of Cs, Ba, U, Pb, and LREE, and low concentrations of HREE, and therefore maybe of cumulate origin. Cumulate dunite containing high-Fo olivine and high-Cr[#] chromite was documented by Arai [60] and Wang et al. [61]. However, the Fo in olivine is uniform, and the relationships between NiO vs. Fo and MnO vs. Fo in olivine do not support a cumulate origin (Figure 6). Chromite inclusions in olivine are common in cumulate dunite, but this is not the case for the studied dunite. Therefore, we discount this possibility.

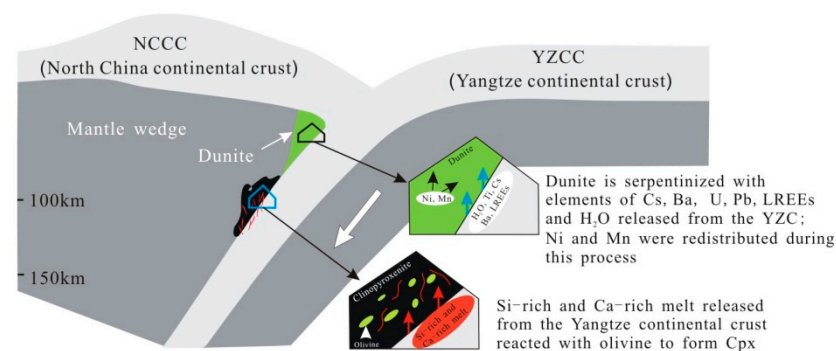
Dunite formed from peridotite-melt interaction commonly contains relics of orthopyroxene [62,63], and shows variable and low Fo in olivine [64]. For the studied dunite, it contains olivine with consistently high Fo, and there are no relics of orthopyroxene. In addition, dunite is large, voluminous, and free of the evidence for melt percolation in the field. Therefore, dunite is likely a residue after partial melting, which is consistent with olivine with high Fo (93.0–94.1) and chromite with high Cr[#] (0.75–0.96).

It is worth noting that the studied dunite shows negatively sloped chondrite-normalized REE patterns (Figures 6 and 10), similar to those of Suoluoshu serpentinite and serpentinite [3]. Considering olivine in residual mantle has low concentrations of REEs, we attribute such negatively sloped REE patterns of the dunite to serpentinization. Serpentinization is also responsible for the low NiO (0.11–0.29 wt.%) and MnO (≤ 0.1 wt.%) contents in olivine, as well as high TiO₂ (up to 0.88 wt.%) in chromite, because these elements are mobile during this alteration [3]. Taken together, dunite is a residue after partial melting and overprinted by aqueous fluids metasomatism.

5.3. Tectonic Evolutions of Hujialin Garnet Clinopyroxenite and Dunite

The tectonic evolution of Hujialin garnet clinopyroxenite has been discussed by many other researchers [5,10,11,15,26,28,65]. They share a common view that Hujialin garnet clinopyroxenite underwent HP-UHP metamorphism during continental collision and subsequently exhumed to the surface with granitic gneisses, but the detailed tectonic evolution of the garnet clinopyroxenite is controversial. Based on our data, we propose the Hujialin garnet clinopyroxenite formed through at least three stages (Figure 11): (1) Clinopyroxenite was formed by interaction of peridotite with a silicic and calcic melt derived from subducted Yangtze continental crust during continental subduction. (2) Clinopyroxenite formed at shallow depths was incorporated into subduction channel and metamorphosed to garnet clinopyroxenite during deep subduction. The P-T conditions of peak metamorphism of the Hujialin garnet clinopyroxenite were estimated at $P \geq 5.0$ GPa, $T \geq 750$ °C [10,26], and 4.5 ± 0.5 GPa, 800 ± 50 °C [5] based on the Mg–Fe exchange of coexisting garnet and clinopyroxene. The conditions are equivalent to a depth of about 150 km. (3) Exhumation to surface occurred. During this stage, retrograded minerals such as amphibole, chlorite, and epidote formed around the garnet at shallow crustal levels (Figure 2c,f,g).

a Formation of clinopyroxenite and hydrated dunite



b Formation of garnet clinopyroxenite and mingled with dunite

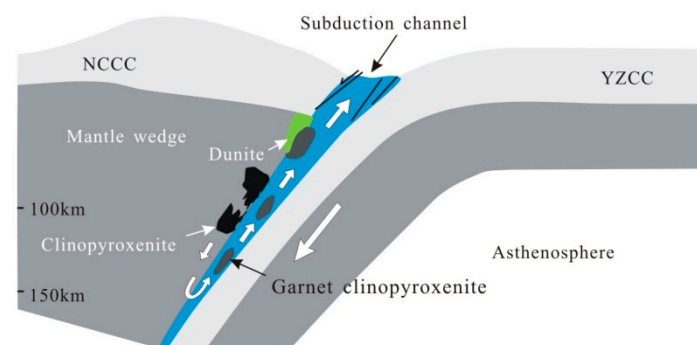


Figure 11. Formation and evolution model for the garnet clinopyroxenite and dunite in Hujialin, Sulu orogen. (a) Formation of the serpentinized dunite and clinopyroxenite. (b) Clinopyroxenite was incorporated into subduction channel and metamorphosed to garnet clinopyroxenite during deep subduction. It mingled with dunite during its exhumation at shallow depths.

Dunite consists of chromite and olivine, and occurs with garnet clinopyroxenite, suggesting two possible paths for it. One possibility is that dunite underwent a deep subduction process. It was incorporated into the subduction channel, and exhumed to the surface later with the garnet clinopyroxenite. The lack of garnet in dunite is likely

attributed to the low content of Al in the bulk rock composition, similar to the dunite in the subduction complex of the northern Dominican Republic [42]. However, we discount this possibility, because serpentine is unstable under HP to UHP conditions [3], and will breakdown, forming secondary forsterite, enstatite, or talc [66]. This is not the case for the studied samples. The dunite is slightly to moderately serpentinized along olivine boundaries and cracks, without secondary forsterite and enstatite. In addition, mineral inclusions in chromite are irregular in shape (Figure 7) and different from those formed under HP to UHP conditions, which tend to be needle-like [67]. Therefore, we propose that dunite was not subjected to deep subduction. Instead, dunite mingled with the garnet clinopyroxenite during the exhumation process of the latter at relatively shallow depths (Figure 11).

6. Conclusions

Mineral chemistry and bulk-rock composition suggest that the precursor of Hujialin garnet clinopyroxenite is clinopyroxenite that formed from the interaction of peridotite with a Si- and Ca- rich melt during subduction of the Yangtze continent beneath the NCC. Dunite is a residue that was overprinted by aqueous fluids.

Clinopyroxenite that formed at shallow depths was incorporated into a subduction channel and transformed to garnet clinopyroxenite during deep subduction. The lack of prograde and retrograde metamorphic minerals in dunite, together with the irregularly shaped mineral inclusions in chromite, indicates that dunite did not subduct to deep levels. Most likely, dunite mingled with garnet clinopyroxenite during exhumation of the latter at relatively shallow depths. These ultramafic rocks, especially hydrated peridotite, may have supplied Au to the Jiaodong Au province [68].

Supplementary Materials: The following supporting information can be downloaded at: <https://www.mdpi.com/article/10.3390/min12020162/s1>, Table S1: Representative composition of clinopyroxene in Hujialin garnet clinopyroxenite (wt.%); Table S2: Representative composition of garnet in Hujialin garnet clinopyroxenite (wt.%); Table S3: Representative composition of olivine in Hujialin dunite (wt.%); Table S4: Representative composition of chromite in Hujialin dunite (wt.%); Table S5: Representative composition of chlorite and epidote in Hujialin clinopyroxenite and dunite (wt.%); Table S6: Representative composition of amphibole and serpentine in Hujialin clinopyroxenite and dunite (wt.%); Table S7: Bulk rock major and minor element compositions of garnet clinopyroxenite and dunite at Hujialin.

Author Contributions: Conceptualization, J.L.; methodology, J.L.; validation, J.W. and K.H.; formal analysis and data curation, J.L. and J.W.; project administration, J.W. and J.L.; writing—original draft, J.L.; field work, J.W. and Z.W. All authors have read and agreed to the published version of the manuscript.

Funding: This research was financially co-supported by the National Natural Science Foundation of China (No. 41472051) to J. Wang and the grant from the Natural Science Foundation of Shandong Province (No. ZR2021QD068) to J.G. Liu.

Data Availability Statement: Not applicable.

Acknowledgments: We thank Zhenyu Chen (Institute of Mineral Resources, Chinese Academy of Geological Sciences) for helping with EPMA analysis. We also thank to the anonymous reviewers who significantly improved the manuscript.

Conflicts of Interest: The authors declare no conflict of interest.

References

1. Zhang, R.Y.; Liou, J.G.; Ernst, W.G. The Dabie-Sulu continental collision zone: A comprehensive review. *Gondwana Res.* **2009**, *16*, 1–26. [[CrossRef](#)]
2. Xie, Z.P.; Hattori, K.; Wang, J. Origins of ultramafic rocks in the Sulu Ultrahigh-pressure Terrane, Eastern China. *Lithos* **2013**, *178*, 158–170. [[CrossRef](#)]

3. Xie, Z.P.; Hattori, K.; Dong, Y.P.; Wang, J. In situ characterization of forearc serpentinized peridotite from the Sulu ultrahigh-pressure terrane: Behavior of fluid-mobile elements in continental subduction zone. *Geosci. Front.* **2021**, *12*, 101139. [[CrossRef](#)]
4. Yang, J.S.; Xu, Z.Q.; Dobrzhinetskaya, L.F.; Green, H.W., II; Pei, X.Z.; Shi, R.D.; Wu, C.L.; Wooden, J.L.; Zhang, J.X.; Wan, Y.S.; et al. Discovery of metamorphic diamonds in central China: An indication of a >4000-km-long zone of deep subduction resulting from multiple continental collisions. *Terra Nova* **2003**, *15*, 370–379. [[CrossRef](#)]
5. Wang, Z.L.; Zhang, S.K.; Li, X.P.; Wang, S.J.; Wang, D.; Kong, F.M.; Liu, J.G.; Li, Z.S.; Li, D.P.; Wang, J.; et al. Metamorphic evolution of garnet-bearing ultramafic rocks in the Hujialin area, Sulu ultrahigh-pressure orogenic belt, Eastern China. *Minerals* **2020**, *10*, 225. [[CrossRef](#)]
6. Zhang, R.Y.; Liou, J.G.; Yang, J.S.; Yui, T.F. Petrochemical constraints for dual origin of garnet peridotites from the Dabie-Sulu UHP terrane, eastern-central China. *J. Metamorph. Geol.* **2000**, *18*, 149–166. [[CrossRef](#)]
7. Xie, Z.P.; Wang, J.; Hattori, K.; Xue, C.D.; Zhong, J.W.; Qang, Z.L. The petrogenesis and tectonic implication of Hujialin ultramafic rocks in the Sulu ultrahigh-pressure metamorphic belt, eastern China. *Acta Petrol. Sin.* **2018**, *34*, 1539–1556, (In Chinese with English Abstract).
8. Zhang, Y.L.; Xu, Y.G. Pyroxenites: High-pressure segregates or recycled oceanic crust? *Geol. J. China Univ.* **2012**, *18*, 74–87, (In Chinese with English Abstract).
9. Li, T.F.; Yang, J.S. Geochemical characteristics of garnet clinopyroxenite at Hujialing, Rizhao, and their bearing on petrogenesis. *Acta Petrol. Mineral.* **2005**, *24*, 469–475, (In Chinese with English Abstract).
10. Yang, J.J. Ca-rich garnet-clinopyroxene rocks at Hujialin in the Su-Lu terrane (eastern China): Deeply subducted arc cumulates? *J. Petrol.* **2006**, *47*, 965–990. [[CrossRef](#)]
11. Xie, Z.P.; Wang, J.; Hattori, K. Cumulates of arc magmas incorporated into the Sulu UHP metamorphic belt, eastern China. *Int. Geol. Rev.* **2016**, *58*, 703–718. [[CrossRef](#)]
12. Li, H.Y.; Chen, R.X.; Zheng, Y.F.; Hu, Z.C. Water in garnet pyroxenite from the Sulu orogen: Implications for crust-mantle interaction in continental subduction zone. *Chem. Geol.* **2018**, *478*, 18–38. [[CrossRef](#)]
13. Zheng, Y.F.; Fu, B.; Gong, B.; Li, L. Stable isotope geochemistry of ultrahigh pressure metamorphic rocks from the Dabie-Sulu orogen in China: Implications for geodynamics and fluid regime. *Earth Sci. Rev.* **2003**, *62*, 105–161. [[CrossRef](#)]
14. Chen, R.X.; Yin, Z.Z.; Xia, C.P. Crustal metasomatism of mantle wedge during collisional orogeny: Insights from orogenic peridotites in the Dabie-Sulu orogenic belt. *Bull. Mineral. Petrol. Geochem.* **2019**, *38*, 459–484, (In Chinese with English Abstract).
15. Zhang, R.Y.; Liou, J.G. Clinopyroxenite from the Sulu ultrahigh-pressure terrane, eastern China: Origin and evolution of garnet exsolution in clinopyroxene. *Am. Mineral.* **2003**, *88*, 1591–1600. [[CrossRef](#)]
16. Zhang, R.Y.; Hirajima, T.; Banno, S.; Cong, B.; Liou, J.G. Petrology of ultrahigh-pressure rocks from the southern Su-Lu region, eastern China. *J. Metamorph. Geol.* **1995**, *13*, 659–675. [[CrossRef](#)]
17. Zheng, Y.F.; Zhou, J.B.; Wu, Y.B.; Xie, Z. Low-grade metamorphic rocks in the Dabie-Sulu orogenic belt: A passive-margin accretionary wedge deformed during continent subduction. *Int. Geol. Rev.* **2005**, *47*, 851–871. [[CrossRef](#)]
18. Zheng, Y.F.; Zhao, Z.F.; Chen, R.X. Ultrahigh-pressure metamorphic rocks in the Dabie-Sulu orogenic belt: Compositional inheritance and metamorphic modification. In *HP-UHP Metamorphism and Tectonic Evolution of Orogenic Belts*; Zhang, L.F., Zhang, Z., Schertl, H.P., Wei, C., Eds.; Geological Society; Special Publications: London, UK, 2019; Volume 474, pp. 89–132.
19. Liu, F.L.; Liou, J.G. Zircon as the best mineral for P-T-time history of UHP metamorphism: A review on mineral inclusions and U-Pb SHRIMP ages of zircons from the Dabie-Sulu UHP rocks. *J. Asian Earth Sci.* **2011**, *40*, 1–39. [[CrossRef](#)]
20. Ye, K.; Cong, B.L.; Ye, D.N. The possible subduction of continental material to depths greater than 200 km. *Nature* **2000**, *407*, 734–736. [[CrossRef](#)]
21. Liu, F.L.; Xu, Z.Q.; Liou, J.G.; Katayama, I.; Masago, H.; Maruyama, S.; Yang, J.S. Ultrahigh-pressure mineral inclusions in zircons from gneissic core samples of the Chinese Continental Scientific Drilling Site in eastern China. *Eur. J. Mineral.* **2002**, *14*, 451–499.
22. Liu, F.L.; Xu, Z.Q.; Yang, J.S.; Zhang, Z.M.; Xue, H.M.; Li, T.F. Geochemical characteristics and UHP metamorphism of granitic gneisses in the main drilling hole of the Chinese Continental Scientific Drilling Project and its adjacent area. *Acta Petrol. Sin.* **2004**, *20*, 9–26, (In Chinese with English Abstract).
23. Yang, J.J.; Jahn, B.M. Deep subduction of mantle-derived garnet peridotites from the Su-Lu UHP metamorphic terrane in China. *J. Metamorph. Geol.* **2000**, *18*, 167–180. [[CrossRef](#)]
24. Liu, F.L.; Xu, Z.Q.; Xue, H.M. Tracing the protolith, UHP metamorphism, and exhumation ages of orthogneiss from the SW Sulu terrane (eastern China): SHRIMP U-Pb dating of mineral inclusion-bearing zircons. *Lithos* **2004**, *78*, 411–429. [[CrossRef](#)]
25. Zong, K.Q.; Liu, Y.S.; Gao, C.G.; Hu, Z.C.; Gao, S.; Gong, H.J. In situ U–Pb dating and trace element analysis of zircons in thin sections of eclogite: Refining constraints on the ultrahigh-pressure metamorphism of the Sulu terrane, China. *Chem. Geol.* **2010**, *269*, 237–251. [[CrossRef](#)]
26. Chen, J.; Xu, Z. Pargasite and ilmenite exsolution texture in clinopyroxenes from Hujialing garnet-pyroxenite, Su-Lu UHP terrane, Central China: A geodynamic implication. *Eur. J. Mineral.* **2005**, *17*, 895–903. [[CrossRef](#)]
27. Gao, T.S.; Chen, J.F.; Xie, Z.; Yang, S.H.; Yu, G. Zircon SHRIMP U-Pb age of garnet olivine pyroxenite at Hujialin in the Sulu terrane and its geological significance. *Chin. Sci. Bull.* **2004**, *49*, 2198–2204. [[CrossRef](#)]
28. Zhao, R.X.; Liou, J.G.; Tsujimori, T.; Zhang, R.Y. Petrology and U-Pb SHRIMP geochronology of a garnet peridotite, Sulu UHP terrane, east-central China. *Int. Geol. Rev.* **2007**, *49*, 732–752. [[CrossRef](#)]

29. Li, T.F.; Yang, J.S.; Zhang, R.Y. Geochemical characteristics and UHP metamorphic age of the Hujialing garnet clinopyroxenite from the Sulu terrane, China and the bearing on its genesis. *Int. Geol. Rev.* **2008**, *50*, 48–60. [[CrossRef](#)]
30. Whitney, D.L.; Evans, B.W. Abbreviations for names of rock-forming minerals. *Am. Mineral.* **2010**, *95*, 185–187. [[CrossRef](#)]
31. Li, M.; Han, Z.Z.; Bi, C.Y.; Zhang, H.; Li, J.R.; Cui, Z.Y. Mineral geochemistry of eclogite in the Sulu belt and its implication. *Period. Ocean Univ. China (Nat. Sci. Ed.)* **2015**, *45*, 63–70. (In Chinese with English Abstract)
32. Feng, P.; Wang, L.; Brown, M.; Johnson, T.M.; Kylander-Clark, A.; Piccoli, P.M. Partial melting of ultrahigh-pressure eclogite by omphacite-breakdown facilitates exhumation of deeply-subducted crust. *Earth Planet. Sci. Lett.* **2021**, *554*, 116664. [[CrossRef](#)]
33. Coleman, R.G.; Lee, D.E.; Beatty, L.B.; Brannock, W.W. Eclogites and eclogites: Their similarities and differences. *Geol. Soc. Am. Bull.* **1965**, *76*, 483–508. [[CrossRef](#)]
34. Morimoto, N. Nomenclature of pyroxenes. *Mineral. Mag.* **1988**, *52*, 535–550. [[CrossRef](#)]
35. Liu, Y.D.; Ying, J.F. Origin of clinopyroxene megacrysts in volcanic rocks from the North China Craton: A comparison study with megacrysts worldwide. *Int. Geol. Rev.* **2019**, *61*, 1–17. [[CrossRef](#)]
36. Xu, W.L.; Zhou, Q.J.; Pei, F.P.; Yang, D.B.; Gao, S.; Li, Q.L.; Yang, Y.H. Destruction of the North China Craton: Delamination or thermal/chemical erosion? Mineral chemistry and oxygen isotope insights from websterite xenoliths. *Gondwana Res.* **2013**, *23*, 119–129. [[CrossRef](#)]
37. Zheng, J.P.; O'Reilly, S.Y.; Griffin, W.L.; Lu, F.X.; Zhang, M.; Pearson, N.J. Relics of refractory mantle beneath the eastern North China Block: Significance for lithosphere evolution. *Lithos* **2001**, *57*, 43–66. [[CrossRef](#)]
38. Zheng, J.P.; Griffin, W.L.; O'Reilly, S.Y.; Yang, J.S.; Li, T.F.; Zhang, M.; Zhang, R.Y.; Liou, J.G. Mineral chemistry of peridotites from Paleozoic, Mesozoic and Cenozoic Lithosphere: Constraints on mantle evolution beneath Eastern China. *J. Petrol.* **2006**, *47*, 2233–2256. [[CrossRef](#)]
39. Ying, J.F.; Zhang, H.F.; Kita, N.; Morishita, Y.; Shimoda, G. Nature and evolution of Late Cretaceous lithospheric mantle beneath the eastern North China Craton: Constraints from petrology and geochemistry of peridotitic xenoliths from Junan, Shandong Province, China. *Earth Planet. Sci. Lett.* **2006**, *244*, 622–638. [[CrossRef](#)]
40. Xu, W.L.; Yang, D.B.; Gao, S.; Pei, F.P.; Yu, Y. Geochemistry of peridotite xenoliths in Early Cretaceous high-Mg# diorites from the Central Orogenic Block of the North China Craton: The nature of Mesozoic lithospheric mantle and constraints on lithospheric thinning. *Chem. Geol.* **2010**, *270*, 257–273.
41. Saumur, B.M.; Hattori, K. Zoned Cr-spinel and ferritchromite alteration in forearc mantle serpentinites of the Rio San Juan Complex, Dominican Republic. *Mineral. Mag.* **2013**, *77*, 117–136. [[CrossRef](#)]
42. Hattori, K.H.; Guillot, S.; Saumur, B.M.; Tubrett, M.N.; Vidal, O.; Morfin, S. Corundum-bearing garnet peridotite from northern Dominican Republic: A metamorphic product of an arc cumulate in the Caribbean subduction zone. *Lithos* **2010**, *114*, 437–450. [[CrossRef](#)]
43. Ozawa, K. Melting and melt segregation in the mantle wedge above a subduction zone: Evidence from the chromite-bearing peridotites of the Miyamori Ophiolite Complex, northeastern Japan. *J. Petrol.* **1994**, *35*, 647–678. [[CrossRef](#)]
44. Nakamura, M. Residence time and crystallization history of nickeliferous olivine phenocrysts from northern Yatsugatake volcanoes, central Japan: Application of a growth and diffusion model in the system Mg-Fe-Ni. *J. Volcanol. Geoth. Res.* **1995**, *66*, 81–100. [[CrossRef](#)]
45. Ishii, T.; Robinson, P.T.; Maekawa, H.; Fiske, R. Petrological studies of peridotites from diapiric serpentinite seamounts in the Izu-Ogasawara-Mariana forearc Leg 125. In *Proceedings of the Ocean Drilling Program Scientific Results*; Fryer, P., Pearce, J.A., Stokking, L.B., Eds.; Ocean Drilling Program: College Station, TX, USA, 1992; Volume 125, pp. 445–485.
46. Parkinson, I.J.; Pearce, J.A. Peridotites from the IzuBonin-Mariana forearc (ODP Leg 125): Evidence for mantle melting and melt-mantle interaction in a supra-subduction zone setting. *J. Petrol.* **1998**, *39*, 1577–1618. [[CrossRef](#)]
47. Hattori, K.H.; Guillot, S. Geochemical character of serpentinites associated with high- to ultrahigh pressure metamorphic rocks in the Alps, Cuba, and the Himalayas: Recycling of elements in subduction zones. *Geochem. Geophys. Geosyst.* **2007**, *8*, Q09010. [[CrossRef](#)]
48. Arai, S.; Okamura, H.; Kadoshima, K.; Tanaka, C.; Suzuki, K.; Ishimaru, S. Chemical characteristics of chromian spinel in plutonic rocks: Implications for deep magma processes and discrimination of tectonic setting. *Isl. Arc* **2011**, *20*, 125–137. [[CrossRef](#)]
49. Enami, M.; Liou, J.G.; Mattinson, C.G. Epidote minerals in high P/T metamorphic terranes: Subduction zone and high- to ultrahigh-pressure metamorphism. *Rev. Mineral. Geochem.* **2004**, *56*, 347–398. [[CrossRef](#)]
50. Hawthorne, F.C.; Oberti, R.; Harlow, G.E.; Maresch, W.V.; Martin, R.F.; Schumacher, J.C.; Welch, M.D. Nomenclature of the amphibole super group. *Am. Mineral.* **2012**, *97*, 2031–2048. [[CrossRef](#)]
51. Gonzaga, R.G.; Lowry, D.; Jacob, D.E.; LeRoex, A.; Schulze, D.; Menzies, M.A. Eclogites and garnet pyroxenites: Similarities and differences. *J. Volcanol. Geoth. Res.* **2010**, *190*, 235–247. [[CrossRef](#)]
52. White, W.M.; Klein, E.M. 4.13-Composition of the oceanic crust. In *Treatise on Geochemistry*, 2nd ed.; Holland, H.D., Turekian, K., Eds.; Elsevier: Oxford, UK, 2014; Volume 4, pp. 457–496.
53. Zhang, H.F.; Ying, J.F.; Shimoda, G.; Kita, N.T.; Morishita, Y.; Shao, J.A.; Tang, Y.J. Importance of melt circulation and crust-mantle interaction in the lithospheric evolution beneath the North China Craton: Evidence from Mesozoic basalt-borne clinopyroxene xenocrysts and pyroxenite xenoliths. *Lithos* **2007**, *96*, 67–89. [[CrossRef](#)]
54. Liu, Y.S.; Gao, S.; Lee, C.T.A.; Hu, S.H.; Liu, X.M.; Yuan, H.L. Melt-peridotite interactions: Links between garnet pyroxenite and high-Mg# signature of continental crust. *Earth Planet. Sci. Lett.* **2005**, *234*, 39–57.

55. Garrido, C.; Bodinier, J.L. Diversity of mafic rocks in the Ronda peridotite: Evidence for pervasive melt/rock reaction during heating of subcontinental lithosphere by upwelling asthenosphere. *J. Petrol.* **1999**, *40*, 729–754. [[CrossRef](#)]
56. McDonough, W.F.; Sun, S.S. The composition of the Earth. *Chem. Geol.* **1995**, *120*, 223–253. [[CrossRef](#)]
57. Yu, S.Y.; Xu, Y.G.; Ma, J.L.; Zheng, Y.F.; Kuang, Y.S.; Hong, L.B.; Ge, W.C.; Tong, L.X. Remnants of oceanic lower crust in the subcontinental lithospheric mantle: Trace element and Sr-Nd-O isotope evidence from aluminous garnet pyroxenite xenoliths from Jiaohe, Northeast China. *Earth Planet. Sci. Lett.* **2010**, *297*, 413–422. [[CrossRef](#)]
58. Kelemen, P.B.; Shimizu, N.; Salters, V.J.M. Extraction of mid-ocean-ridge basalt from the upwelling mantle by focused of melt in dunite channels. *Nature* **1995**, *375*, 747–753. [[CrossRef](#)]
59. Kelemen, P.B. Reaction between ultramafic rock and fractionating basaltic magma I. Phase relations, the origin of calc-alkaline magma series, and the formation of discordant dunite. *J. Petrol.* **1990**, *31*, 51–98. [[CrossRef](#)]
60. Arai, S. Characterization of spinel peridotites by olivine-spinel compositional relationships: Review and interpretation. *Chem. Geol.* **1994**, *113*, 191–204. [[CrossRef](#)]
61. Wang, J.; Hattori, K.; Xu, W.L.; Yang, Y.Q.; Xie, Z.P.; Liu, J.L.; Song, Y. Origin of ultramafic xenoliths in high-Mg diorites from east-central China based on their oxidation state and abundance of platinum group elements. *Int. Geol. Rev.* **2012**, *54*, 1203–1218. [[CrossRef](#)]
62. Su, B.X.; Zhou, M.F.; Robinson, P.T. Extremely large fractionation of Li isotopes in a chromitite-bearing mantle sequence. *Sci. Rep.* **2016**, *6*, 22370. [[CrossRef](#)]
63. Xiong, F.H.; Yang, J.S.; Xu, X.Z.; Kapsiotis, A.; Hao, X.L.; Liu, Z. Compositional and isotopic heterogeneities in the Neo-Tethyan upper mantle recorded by coexisting Al-rich and Cr-rich chromitites in the Purang peridotite massif, SW Tibet China. *J. Asian Earth Sci.* **2018**, *159*, 109–129. [[CrossRef](#)]
64. Wang, J.; Hattori, K.; Stern, C.R. Metasomatic origin of garnet orthopyroxenites in the subcontinental lithospheric mantle underlying Pali Aike volcanic field, Southern South America. *Mineral. Petrol.* **2008**, *94*, 243–258. [[CrossRef](#)]
65. Hiramatsu, N.; Hirajima, T. Petrology of the Hujialin garnet clinopyroxenite in the Su-Lu ultrahigh pressure province, eastern China. *Isl. Arc* **1995**, *4*, 310–323. [[CrossRef](#)]
66. Wunder, B.; Wirth, R.; Gottschalk, M. Antigorite: Pressure and temperature dependence of polysomatism and water content. *Eur. J. Mineral.* **2001**, *13*, 485–495. [[CrossRef](#)]
67. Arai, S. Possible recycled origin for ultrahigh-pressure chromitites in ophiolites. *J. Mineral. Petrol. Sci.* **2010**, *105*, 280–285. [[CrossRef](#)]
68. Groves, D.I.; Santosh, M. The giant Jiaodong gold province: The key to a unified model for orogenic gold deposits? *Geosci. Front.* **2016**, *7*, 409–417. [[CrossRef](#)]